Jeon, Junmo; Lindberg, Daniel

Thermodynamic optimization and phase equilibria study of the MgO–ZnO, CaO–ZnO, and CaO–MgO–ZnO systems

Published in:
Ceramics International

DOI:
10.1016/j.ceramint.2022.12.138

Published: 15/04/2023

Document Version
Publisher's PDF, also known as Version of record

Please cite the original version:
Jeon, J., & Lindberg, D. (2023). Thermodynamic optimization and phase equilibria study of the MgO–ZnO, CaO–ZnO, and CaO–MgO–ZnO systems. *Ceramics International*, *49*(8), 12736-12744.
https://doi.org/10.1016/j.ceramint.2022.12.138

Ceramics International 49 (2023) 12736–12744

Contents lists available at ScienceDirect

Ceramics International

journal homepage: www.elsevier.com/locate/ceramint

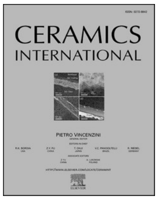

Thermodynamic optimization and phase equilibria study of the MgO–ZnO, CaO–ZnO, and CaO–MgO–ZnO systems

Junmo Jeon, Daniel Lindberg *

Aalto University, School of Chemical Engineering, Department of Chemical and Metallurgical Engineering, P.O. Box 16100, 00076, Aalto, Finland

ARTICLE INFO

Keywords:
Thermodynamic modeling
Phase equilibria
Metallurgical slags
Refractories

ABSTRACT

The binary MgO–ZnO and CaO–ZnO systems and the ternary CaO–MgO–ZnO system were thermodynamically optimized with phase equilibria studies in this study. Bragg-Williams random mixing model was used for solid solutions, while Modified Quasichemical Model was used for liquid solution. The thermodynamic optimization was conducted using Factsage 8.1 thermochemical software. The optimized phase diagrams fit well with phase equilibria experimental results. The phase equilibria studies were performed for the MgO–ZnO systems at 600 °C, 650 °C, 700 °C, and 1000 °C, and for CaO–MgO–ZnO systems at 1500 °C, 1550 °C, and 1600 °C. Quenched samples were analyzed by SEM/EDS to confirm equilibrium phases. Liquid phases were newly observed in the CaO–MgO–ZnO systems at 1550 °C and 1600 °C.

1. Introduction

Multifarious materials have been widely required in manufacturing industries to enhance or alternate major materials in their fields. Calcium oxide (CaO), magnesium oxide (MgO), and zinc oxide (ZnO) have recently been in the spotlight in the semiconductor fields with their structural, electronic and optical properties [1–3]. CaO, MgO, and ZnO are also considered as prospective materials for the solar cells [4–6]. In high entropy oxides (HEOs) fields, MgO and ZnO have been in focus. Although solid MgO and ZnO have different crystal structures (MgO, CaO: cubic halite structure, cF8, space group $F3\overline{m}3$; ZnO: wurtzite structure, hP4, space group $P6_3mc$) they can form extensive solid solutions, e.g. $Mg_{0.2}Zn_{0.2}Co_{0.2}Cu_{0.2}Ni_{0.2}O$ [7,8]. Moreover, CaO and MgO have a high melting point and high resistance to slag penetration at high temperature, thus they are broadly used as refractory materials in the pyrometallurgy fields [9].

CaO, MgO, and ZnO materials can be recovered from pyrometallurgical slags [10–12]. Copper smelting slag can be considered as a resource because it includes CaO, MgO, and ZnO [13,14]. In the copper smelting process, slags are commonly in liquid state at the process conditions. Therefore, there are challenges to predict the behavior of the liquid slag at high temperature. ZnO from the liquid slag can react with refractories, while MgO from refractories can be dissolved into the liquid slag [13]. CaO concentration in the slag also can influence the slag - matte equilibria during the processes [15]. Hence, investigation of phase equilibria and thermodynamic predictions for the behavior of liquid slags is needed to understand the effect of CaO, MgO, and ZnO on refractory and slag behavior in pyrometallurgical processes, as well as the interaction with liquid metals and mattes in these processes.

The slags in copper/non-ferrous smelting and refining are multi-component systems containing CaO, MgO, ZnO, CuO_x, FeO_x, Al_2O_3, and SiO_2, as well as other minor oxides, and sulfides [13,14]. In order to understand the chemistry of complex slag systems, thermodynamic modeling can be used to predict melting behavior, slag-refractory, and slag/matte/metal interactions and elemental distribution between phases. Multicomponent, multiphase thermodynamic modeling is typically based on Gibbs energy minimization techniques, and suitable software, such as Factsage, Thermo-Calc or MTDATA is required for such calculations. In addition, thermodynamic databases are required to describe thermodynamic properties of the phases included in the predictions. Development of these databases are based on the so-called Calphad Methodology, which is a methodology to assess and optimize thermodynamic properties of phases, and especially non-ideal interaction parameters of solution phases, such as liquids and solid solutions, based on experimental phase equilibrium and thermodynamic data [16,17]. Typically, lower order systems (unary & binary systems) are optimized before optimizing higher order systems. Therefore, the binary system, such as MgO–ZnO, CaO–ZnO, and CaO–MgO systems can be considered for the first step before optimizing the ternary CaO–MgO–ZnO system. According to previous phase equilibria studies,

---

* Corresponding author.
E-mail address: daniel.k.lindberg@aalto.fi (D. Lindberg).

https://doi.org/10.1016/j.ceramint.2022.12.138
Received 16 September 2022; Received in revised form 25 November 2022; Accepted 14 December 2022

the phase equilibria of MgO–ZnO [18–22] and CaO–ZnO [23] systems were determined with their solid solubility [18–23], eutectic point, liquidus and solidus line [23]. They also suggested potential phase diagrams of the binary systems. Moreover, the thermodynamic optimizations of the CaO–ZnO [24] and CaO–MgO [25] system were performed with phase equilibria studies. For the binary CaO–ZnO and MgO–ZnO systems as well as the ternary CaO–MgO-ZnO system, the Gibbs energies of the metastable form of CaO and MgO in Zincite (wurtzite structure), and ZnO in monoxide phase (halite structure) were comprehensively considered in this study, thus the CaO–ZnO system was reoptimized to be consistent with the ternary CaO–MgO–ZnO system. For the next step, the ternary systems can be considered, such as the CaO–MgO–ZnO system. If the experimental data in binary system is scarce and several non-unique sets of parameters may be produced to fit the same data, it may also be useful to conduct simultaneous optimization of binary and ternary systems in order to find a unique set of parameters for the binary systems and reduce the use of ternary parameters [26].

In this study, the focus was on the binary MgO–ZnO, CaO–ZnO systems and ternary CaO–MgO–ZnO system with phase equilibria experiments and thermodynamic optimization using Factsage 8.1 thermochemical software [27]. FToxid database from the Factsage 8.1 was used for values of standard state of MgO, ZnO, and CaO. For solid solution phases, Bragg-Wiliams random mixing model was used, while Modified Quasichemical Model was used for liquid solution phases [28–30].

2. Model theory

When more than two different elements are mixing to become solutions, they show two cases of behaviors: 1) Ideal solution, where the components are mixed randomly and enthalpy and volume of mixing are zero, and 2) Non-ideal solution has excess Gibbs energy for mixing due to their positive or negative interaction within each component. For solution phases, the Gibbs energy of the solution can be expressed by equation (1):

$$G^{solution} = G^o + \Delta G_{mix}^{ideal} + \Delta G_{mix}^{excess}$$

$$= G^o + \left(-T\Delta S_{mix}^{configural}\right) + \Delta G_{mix}^{excess} \tag{1}$$

Where G^o is a pure Gibbs energy of components, and ΔG_{mix}^{ideal} is an ideal mixing Gibbs energy for ideal solution. $\Delta S_{mix}^{configural}$ is a configurational entropy of mixing. ΔG_{mix}^{excess} is excess Gibbs energy for regular solution, and its several model equations were mentioned in previous studies [28–30]. In this study, the Bragg-Williams random mixing model (BW) and Modified Quasichemical Model (MQM) were used.

ΔG_{mix}^{excess} of the binary MgO–ZnO, CaO–ZnO, and ternary CaO–MgO–ZnO solid solutions were calculated using the Bragg-Williams model. This model is considering random mixing of components, thus an ideal configurational entropy of mixing, $\Delta S_{mix}^{configural,ideal}$ is introduced as shown in equation (2). Moreover, ΔG_{mix}^{excess} can be expressed as a polynomial function in the binary solutions in real system with empirical parameters using equation (3) for the binary MgO–ZnO and CaO–ZnO solutions [30].

$$\Delta S_{mix}^{configural,ideal} = -\mathrm{R}\sum n_e ln x_e \ (\mathrm{e = element}) \tag{2}$$

$$\Delta G_{mix}^{excess} = \Delta g_{AB} = \sum q_{AB}^{ij} Y_A^i Y_B^j \quad (\mathrm{i\,,j} \geq 0) \tag{3}$$

$$Y_A = \frac{Z_A X_A}{Z_A X_A + Z_B X_B}\ , Y_B = \frac{Z_B X_B}{Z_A X_A + Z_B X_B}$$

Where q is parameter, Z is coordination number, and Y is coordination-equivalent fractions.

For the ternary CaO–MgO–ZnO solution, ΔG_{mix}^{excess} can be expressed as a polynomial function following equation (4)

$$\Delta G_{mix}^{excess} = \Delta g_{ABC} = \sum q_{ABC}^{ijk} Y_A^i Y_B^j Y_C^k \left(\mathrm{i, j, k} \geq 1, \frac{Y_A}{Y_B}, \frac{Y_A}{Y_C}, or \frac{Y_B}{Y_C} = constant\right) \tag{4}$$

$$Y_A = \frac{Z_A X_A}{Z_A X_A + Z_B X_B + Z_C X_C}\ , Y_B = \frac{Z_B X_B}{Z_A X_A + Z_B X_B + Z_C X_C}, Y_C = \frac{Z_C X_C}{Z_A X_A + Z_B X_B + Z_C X_C}$$

Meanwhile, ΔG_{mix}^{excess} of the binary MgO–ZnO and CaO–ZnO liquid solution systems were calculated using Modified Quasichemical Model. This model is considering Short Range Order (SRO), such as (A-A), (B–B), and (A-B) pairs [28,29]. Therefore, configurational entropy of mixing that can express SRO is introduced as shown in equation (5). Also, ΔG_{mix}^{excess} can be expressed as a polynomial function in the binary solutions in real system with empirical parameters using equation (6) [30].

$$\Delta S_{mix}^{configural,MQM} = -R(n_A ln x_A + n_B ln x_B) - R\left[n_{AA}\ \mathrm{ln}\left(\frac{X_{AA}}{Y_A^2}\right) + n_{BB}\ \mathrm{ln}\left(\frac{X_{BB}}{Y_B^2}\right) + n_{AB}\ \mathrm{ln}\left(\frac{X_{AB}}{2Y_A Y_B}\right)\right] \tag{5}$$

$$\Delta G_{mix}^{excess} = (n_{AB}/2)\,\Delta g_{AB}, \Delta g_{AB} = \sum q_{AB}^{ij} Y_A^i Y_B^j \quad (\mathrm{i, j} \geq 0) \tag{6}$$

Where $n_{AA,BB,AB}$ is mole of pairs, $X_{AA,BB,AB}$ is pair fraction, and $Y_{A,B}$ is coordination-equivalent fractions. If there is no Short Range Order (SRO) by $X_{AA} = Y_A^2, X_{BB} = Y_B^2, and\, X_{AB} = 2Y_A Y_B$, then the $\Delta S_{mix}^{configural}$ shows ideal random mixing behavior as the Bragg-Williams model, –R $\sum n_e ln x_e$.

3. Experimental

For phase equilibria studies of the binary MgO–ZnO and ternary CaO–MgO–ZnO systems, several types of mixtures were prepared. For experiments at very high temperatures, the mixtures consisted of the pure oxides (MgO–ZnO and CaO–MgO–ZnO mixtures), while for experiments at lower temperatures, additional components were used to produce conditions where a liquid phase was formed during the experiment. The purpose to form a liquid phase was to facilitate mass transfer of Mg^{2+} and Zn^{2+} via the liquid phase to the solid solutions, and reach equilibrium at shorter times compared to solid-solid equilibria. The additional components were chosen so that they would not dissolve into either MgO(ss) or ZnO(ss), and the mixture compositions were chosen to give an equilibrium phase assemblage where both MgO(ss) and ZnO(ss) were present, together with other solid or liquid phases. The additional components were either P_2O_5 or a mixture of metallic Mg and Zn due to their low melting points. MgO (99.95%, Alfa Aesar), ZnO (99.99%, Alfa Aesar), and CaO (99.9%, Sigma Aldrich) powders were used. They were dried at 110 °C for 24 h and ground with a mortar. P_2O_5 powder (99%, Sigma Aldrich), Mg turning (99.98%, Alfa Aesar) and Zn shot (99.999%, Alfa Aesar) were also used to suppress and/or offset vaporization of Zn during experiments. For the binary MgO–ZnO system, Mg–ZnO–Zn and MgO–ZnO–P_2O_5 mixtures (~0.5g) were prepared, while CaO–MgO–ZnO mixtures (~0.15g) were prepared for the ternary CaO–MgO–ZnO system. All mixtures were pelletized as a cylinder shape with a 5 mm diameter. In order to contain the pellets, MgO crucible & lid was prepared for the MgO–ZnO system. Pt crucible & lid was also prepared for the CaO–MgO–ZnO system. The Mg–ZnO–Zn and MgO–ZnO–P_2O_5 mixture compositions and temperatures were chosen to produce equilibrium mixtures where MgO(ss), ZnO(ss) and a liquid phase are in equilibrium with each other, in order to produce conditions with MgO (ss) in equilibrium with ZnO(ss) with the liquid phase acting as a facilitator for reaching of equilibrium within reasonable times. The compositions of pellets and a type of crucibles are shown in Table 1.

The phase equilibria experiments were conducted using a vertical

Table 1
Initial composition of pellets and experimental conditions for phase equilibria studies.

No.	System	Initial composition (Mole ratio)	Crucible & Lid	Temp. (^oC)	Time (Hours)	Atmosphere
1	MgO–ZnO	0.05Mg-0.95ZnO–Zn[a]	MgO	600	24	Ar
2					48	
3				650	48	
4				700	24	
5		0.3MgO-0.6ZnO-0.1P_2O_5		1000	24	Air
6		0.45MgO-0.45ZnO-0.1P_2O_5				
7	CaO–MgO–ZnO	0.45CaO-0.45MgO-0.1ZnO	Pt	1500	10	Air
8		0.375CaO-0.375MgO-0.25ZnO				
9		0.02CaO-0.35MgO-0.63ZnO				
10		0.4CaO-0.05MgO-0.55ZnO				
11		0.3CaO-0.2MgO-0.5ZnO		1500	10	
12		0.1CaO-0.2MgO-0.7ZnO				
13				1550		
14						
15				1600	6	
16						

[a] 0.05–0.1g added to offset Zn vaporization.

tube furnace as shown in Fig. 1. For the binary MgO–ZnO system, Mg–ZnO–Zn pellets were used at 600, 650, and 700 °C experiments at 99.999%Ar atmosphere for 24 and/or 48 h. MgO–ZnO–P_2O_5 pellets were used for 1000 °C experiments at air atmosphere for 24 h. For the ternary CaO–MgO–ZnO system, the CaO–MgO–ZnO pellets were used at 1500, 1550, and 1600 °C at air atmosphere for 6 and/or 10 h. The experimental conditions are shown in Table 1. Each sample was put into a crucible covered with a lid. A Pt wire was used to hang the sample, and the sample was located in a hot zone of the furnace at a targeted temperature and atmosphere. Also, a tip of the S-type thermocouple was placed next to the sample during equilibria experiments. The equilibria experiment time was determined by referring to previous studies [18, 23]. When the equilibrium time was reached, the sample was dropped down into ice water in a moment for quenching. After that, the sample was immediately dried and cold-mounted.

The mounted samples were cut and polished until 5 μm to observe cross-sections. Scanning Electron Microscope (SEM) and Energy Dispersive Spectroscopy (EDS) were used to determine and clarify phase equilibria. Backscattered electrons (BSE) mode of SEM was used to distinguish phases. The standards of Ca, Mg, Zn, P, and O elements were considered for EDS analysis to increase reliability. The standards were fluorite (Ca Kα), metallic zinc and magnesium (Mg Kα and Zn Kα), apatite (P Kα), and quartz (O Kα). With the SEM/EDS results, the thermodynamic optimizations of phase diagram for MgO–ZnO system and CaO–MgO–ZnO ternary system were performed utilizing Solution and OptiSage functions of Factsage 8.1, thermochemical software, covering Bragg-Williams model and Modified Quasichemical model [28–30].

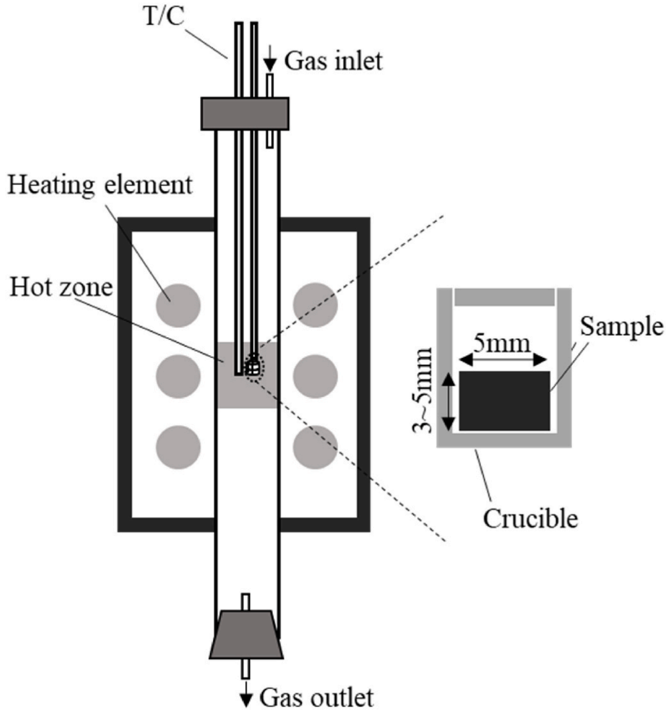

Fig. 1. Apparatus for phase equilibria study.

4. Results and discussion

4.1. The binary MgO–ZnO and CaO–ZnO systems

Phase equilibria studies of the binary MgO–ZnO system were designed to figure out solubilities of components to phases, such as a MgO solubility in zincite and ZnO solubility in monoxide. The initial compositions of sample and are shown in Table 1 (Experimental No. 1 to 6). The result compositions of solubilities are shown in Table 2, as well as the results were marked on the MgO–ZnO phase diagram as shown in Fig. 3.

Fig. 2 shows SEM images of phase equilibria on the MgO–ZnO system at 600, 650, 700, and 1000 °C, respectively. In the all-targeted temperature range, two equilibria phases separately existed as monoxide and zincite structures in the MgO–ZnO system. The darker area indicates a monoxide phase, while the brighter area is a zincite phase. The black area is an empty space that used to include vaporized Zn metals. The solubilities of MgO and ZnO were shown in Table 2, and Fig. 3 visibly shows the results with symbols. ZnO solubility in monoxide was gradually increased from 600 to 1000 °C. Its tendency followed well the results of L.Xia et al. [18] Meanwhile, MgO showed less solubility in zincite until 700 °C. However, the solubility was increased at 1000 °C, and it also showed following well the previous studies [18,21].

As shown in Fig. 3, the optimized phase diagram of MgO–ZnO system was calculated using Factsage, based on present and previous phase equilibria studies [18–22]. The values of optimized parameters are shown in Table 3. For the entire MgO–ZnO solution, the metastable Gibbs energies, $\Delta G^{metastable}$ of MgO in zincite (MgO(monoxide)→MgO (zincite)) and of ZnO in monoxide (ZnO(zincite)→ZnO(monoxide)), were calculated utilizing OptiSage function applied by Nonlinear Optimization with Mesh Adaptive Direct search algorithm, NOMAD [31] and Bayesian [32] methods. For the solid solution, the parameters of MgO–ZnO in monoxide and zincite phases were calculated using the Bragg-Williams model with polynomial equation (3), while the parameters of MgO–ZnO in the liquid solution were calculated using the Modified Quasichemical Model with polynomial equation (6). The new

Table 2
EDS results of phase equilibria studies of the MgO–ZnO and CaO–MgO–ZnO systems.

No.	System	Temp.,°C	Time,hrs	Phase	Components (mol%)		
					CaO	MgO	ZnO
1	MgO–ZnO	600	24	Monoxide	–	85.4 ± 0.7	14.6 ± 0.7
				Zincite		0	100
2			48	Monoxide		86.0 ± 0.7	14.0 ± 0.7
				Zincite		0.1 ± 0.1	99.9 ± 0.1
3		650	48	Monoxide		85.9 ± 0.4	14.1 ± 0.4
				Zincite		0.1 ± 0.2	99.9 ± 0.2
4		700	24	Monoxide		84.4 ± 0.4	15.6 ± 0.4
				Zincite		0.1 ± 0.2	99.9 ± 0.2
5		1000[a]	24	Monoxide		76.1 ± 1.7	23.9 ± 1.7
				Zincite		5.7 ± 2.4	94.3 ± 2.4
6			24	Monoxide		77.5 ± 2.7	22.5 ± 2.7
				Zincite		6.2 ± 2.2	93.8 ± 2.2
7	CaO–MgO–ZnO	1500	10	Monoxide#1	1.3 ± 0.3	81.3 ± 1.0	17.4 ± 0.9
				Monoxide#2	93.4 ± 0.4	2.8 ± 0.4	3.8 ± 0.2
8				Monoxide#1	2.8 ± 0.3	61.6 ± 1.2	35.6 ± 1.2
				Monoxide#2	87.1 ± 0.4	2.9 ± 0.1	10.0 ± 0.4
9				Monoxide#1	1.5 ± 0.1	54.3 ± 0.4	44.2 ± 0.3
				Zincite	1.6 ± 0.1	15.3 ± 0.8	83.1 ± 0.8
10				Monoxide#2	82.8 ± 0.3	1.1 ± 0.1	16.1 ± 0.3
				Zincite	4.7 ± 0.6	5.7 ± 0.4	89.6 ± 0.8
11		1500	10	Monoxide#1	5.6 ± 0.2	47.8 ± 0.5	46.6 ± 0.4
				Monoxide#2	74.9 ± 0.3	4.5 ± 0.2	20.6 ± 0.3
				Zincite	4.0 ± 0.3	14.1 ± 2.2	81.9 ± 2.1
12				Monoxide#1	5.3 ± 0.2	47.8 ± 0.7	46.9 ± 0.8
				Monoxide#2	74.1 ± 0.4	4.5 ± 0.2	21.4 ± 0.4
				Zincite	3.8 ± 0.1	15.3 ± 0.9	80.9 ± 0.9
13		1550		Monoxide#1	6.6 ± 1.2	45.2 ± 0.7	48.2 ± 0.8
				Monoxide#2	68.6 ± 0.3	5.6 ± 0.2	25.8 ± 0.3
				Zincite	5.1 ± 2.0	13.5 ± 2.4	81.4 ± 1.4
14				Monoxide#1	5.9 ± 0.2	45.6 ± 0.7	48.5 ± 0.6
				Monoxide#2	67.6 ± 0.5	5.6 ± 0.4	26.8 ± 0.6
				Zincite	3.8 ± 0.2	15.1 ± 0.5	81.1 ± 0.5
15		1600	6	Monoxide#1	7.4 ± 0.3	45.8 ± 0.6	46.8 ± 0.4
				Monoxide#2	60.1 ± 2.3	9.1 ± 1.1	30.8 ± 1.5
				Slag	37.4 ± 1.4	5.5 ± 1.5	57.1 ± 1.5
16				Monoxide#1	7.5 ± 0.2	44.6 ± 0.5	47.9 ± 0.5
				Monoxide#2	64.4 ± 3.4	8.0 ± 0.7	27.6 ± 2.8
				Slag	36.0 ± 1.4	5.1 ± 0.7	58.9 ± 1.6

[a] Contents P_2O_5 of in both monoxide and zincite were less than 0.1 mol% at 1000 °C.

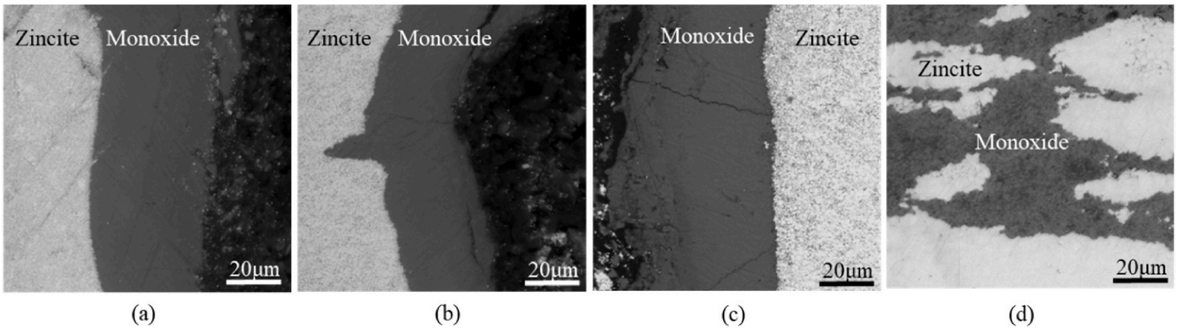

(a) (b) (c) (d)

Fig. 2. SEM image of phase equilibria of the binary MgO–ZnO systems (a) at 600 °C (b) at 650 °C (c) at 700 °C (d) at 1000 °C.

optimized phase diagram of MgO–ZnO shows that it fits well the phase equilibria studies of both present and previous studies from 600 °C to 1600 °C. Meanwhile, Fig. 4 shows the activities of MgO against the mole fraction of MgO in the MgO–ZnO system at 920 °C and 1000 °C. The activities of MgO were measured using a solid-state galvanic cell [21]. The new optimized lines from this study show that they fit well with the experimental data of MgO activity at 920 °C and 1000 °C. It can indicate that it increases the reliability of the new optimized parameters.

The optimized phase diagram of the CaO–ZnO system is shown in Fig. 5. The thermodynamic calculation was conducted based on previous phase equilibria studies [23,24]. In the previous studies, the experiments were carried out from 1000 °C to 1600 °C. The eutectic point was determined at 1535 °C. Liquidus and solidus lines were also determined from phase equilibria results at 1575 °C and 1600 °C. For optimization of the CaO–ZnO phase diagram, the metastable Gibbs energy, $\Delta G^{metastable}$ of CaO in zincite was also calculated utilizing OptiSage function. The $\Delta G^{metastable}$ of ZnO in monoxide is the same as the above of MgO–ZnO system. Bragg-Wiliams model and polynomial equation (3) were used to calculate parameters of CaO–ZnO in monoxide and zincite phases, while parameters of CaO–ZnO in the liquid solution were calculated using the Modified Quasichemical Model and polynomial equation (6). The values of the parameter are shown in Table 3. The new optimized phase diagram of CaO–ZnO can describe the existence of zincite phase and fits well the phase equilibria studies, such as solid

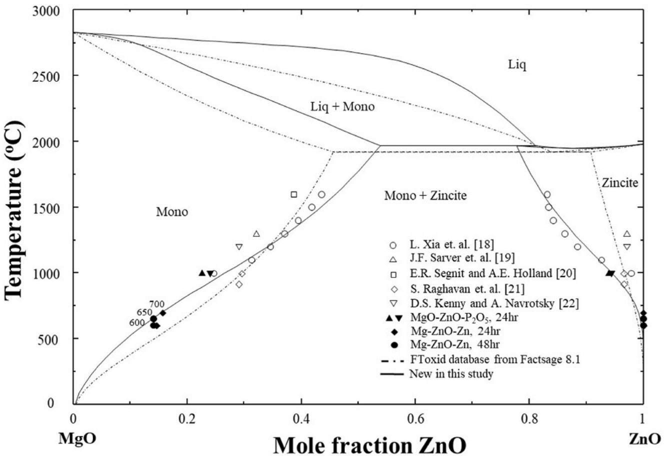

Fig. 3. Optimized phase diagram of the binary MgO–ZnO system. Experimental data from this study, L.Xia et al. [18], J.F. Sarver et al. [19], E.R. Segnit and A. E. Holland [20], S. Raghavan et al. [21], and D.S. Kenny and A. Navrotsky [22].

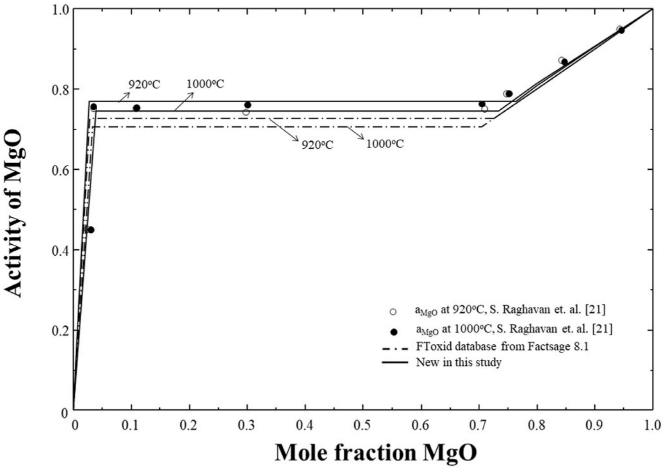

Fig. 4. Optimized MgO activities graph of the binary MgO–ZnO system at 920 °C and 1000 °C. Experimental data from Raghavan et al. [21].

Table 3
Thermodynamic properties of components and parameters of mixing of excess Gibbs energy.

Component	T range (K)	$\Delta H^o_{298.15K}$ $(J \bullet mol^{-1})$	$S^o_{298.15K}$ $(J \bullet mol^{-1}K^{-1})$	$C_p (J \bullet mol^{-1}K^{-1})$
CaO (s, monoxide)	298.15 to 2845.16	−635090.0	37.7500	58.791170568–1147145.98248 T^{-2} -133.903999616 $T^{-0.5}$ +102978787.864 T^{-3}
CaO (l)	298.15 to 2845.16	−555594.0	65.6908	58.791170568–1147145.98248 T^{-2} -133.903999616 $T^{-0.5}$+102978787.864 T^{-3}
MgO (s, monoxide)	298.15 to 3097.91	−601500.0	26.9514	61.109650488–621154.00408 T^{-2} -296.19899984 $T^{-0.5}$ +5844612.0272 T^{-3}
MgO (l)	298.15 to 3097.91	−545345.0	27.0040	72.795562488–0.003142184 T + 522751.59592 T^{-2} -296.19899984 $T^{-0.5}$ +5844612.0272 T^{-3}
ZnO (s, zincite)	298.15 to 2248	−350460.0	43.6390	48.24152 + 0.006794816 T −103768354.688 T^{-3} -91.547409504 $T^{-0.5}$
ZnO (l)	298.15 to 2248	−296068.0	67.8350	48.24152 + 0.006794816 T −103768354.688 T^{-3} -91.547409504 $T^{-0.5}$
CaO (s, zincite)	298.15 to 2845.16	−551991.3	59.6642	58.791170568–1147145.98248 T^{-2} -133.903999616 $T^{-0.5}$ +102978787.864 T^{-3}
MgO (s, Zincite)	298.15 to 3097.91	−565500.0	30.9514	61.109650488–621154.00408 T^{-2} -296.19899984 $T^{-0.5}$ +5844612.0272 T^{-3}
ZnO (s, monoxide)	298.15 to 2248	−317332.0	54.6705	48.24152 + 0.006794816 T −103768354.688 T^{-3} -91.547409504 $T^{-0.5}$

	Component	Phase	**Parameters** $(J \bullet mol^{-1}$ or $J \bullet mol^{-1}K^{-1})$
$\Delta G^{metastable}$	CaO	Zincite	83098.7–21.9142 T
	MgO	Zincite	36000.0–4 T
	ZnO	Monoxide	33128.0–11.0315 T

Phase	**Model**	q^{ij}_{AB} or q^{ijk}_{ABC} *	**Parameters** $(J \bullet mol^{-1}$ or $J \bullet mol^{-1}K^{-1})$
Monoxide	Bragg-Williams	$q^{11}_{MgO,ZnO}$	−14000.5 -2.15 T
		$q^{21}_{MgO,ZnO}$	−6500.55 + 15.15 T
		$q^{11}_{CaO,ZnO}$	20000 -9 T
		$q^{21}_{CaO,ZnO}$	29500 -6 T
		$q^{11}_{CaO,MgO}$	118110–18.41 T [25]
		$q^{21}_{CaO,MgO}$	−31380 [25]
		$q^{111}_{CaO,MgO,ZnO}$	155500 -87 T
Zincite	Bragg-Williams	$q^{11}_{MgO,ZnO}$	9500–3.5 T
		$q^{12}_{MgO,ZnO}$	26000–28.5 T
Liquid	Modified Quasi-chemical Model	Coordination number, Z: $Z^{Ca^{2+}}_{Ca^{2+},Ca^{2+}} = Z^{Zn^{2+}}_{Zn^{2+},Zn^{2+}} = Z^{Mg^{2+}}_{Mg^{2+},Mg^{2+}}$ $= Z^{Ca^{2+}}_{Ca^{2+},Zn^{2+}} = Z^{Ca^{2+}}_{Ca^{2+},Mg^{2+}}$ $= Z^{Zn^{2+}}_{Zn^{2+},Ca^{2+}} = Z^{Zn^{2+}}_{Zn^{2+},Mg^{2+}}$ $= Z^{Mg^{2+}}_{Mg^{2+},Ca^{2+}} = Z^{Mg^{2+}}_{Mg^{2+},Zn^{2+}}$ $= 1.3774$	
		$q^{00}_{Ca^{2+},Zn^{2+}}$	−23700
		$q^{01}_{Ca^{2+},Zn^{2+}}$	−30000
		$q^{00}_{Mg^{2+},Zn^{2+}}$	50000
		$q^{01}_{Mg^{2+},Zn^{2+}}$	−56000
		$q^{02}_{Mg^{2+},Zn^{2+}}$	−55000
		$q^{00}_{Ca^{2+},Mg^{2+}}$	45329 [25]
		$q^{10}_{Ca^{2+},Mg^{2+}}$	−30583 [25]

* $\Delta G^{excess}_{mix} = \sum q^{ij}_{AB} Y^i_A Y^j_B$, or $\sum q^{ijk}_{ABC} Y^i_A Y^j_B Y^i_C$
**The values of $\Delta G^o_{MgO,ZnO,or\ CaO}$ were used from FToxid database, Factsage8.1.

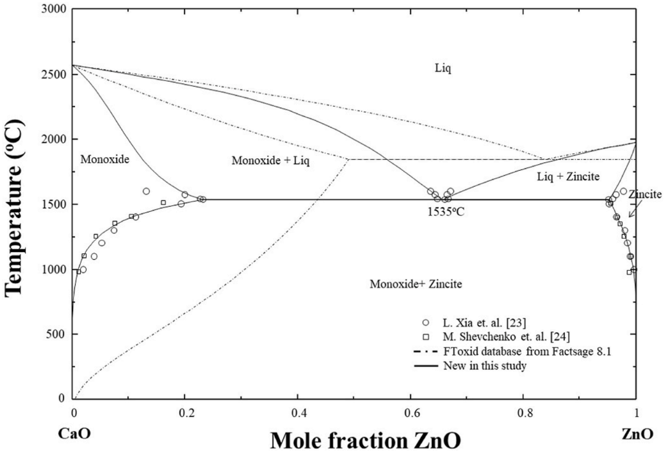

Fig. 5. Optimized phase diagram of the binary CaO–ZnO system. Experimental data from L.Xia et al. [23] and M.Shevchenko et al. [24].

solubilites [23,24], eutectic point at 1535 °C, and solidus & liquidus lines [23].

4.2. *The ternary CaO–MgO–ZnO system*

The experimental phase equilibria of the ternary CaO–MgO–ZnO system was studied to identify phase compositions in two- and three phase equilibria at 1500, 1550, and 1600 °C. The initial compositions were set in triangle area on expected phase diagrams as shown in Table 1 (Experimental No. 11 to 16). They also were visibly marked as opened symbols as shown in Figs. 8–10. Furthermore, additional experiments were performed to figure out equilibrium lines at 1500 °C. The initial compositions were shown in Table 1 (Experimental No. 7 to 10), as well as marked as opened symbols, in the quadrangle areas as shown in Fig. 8. The results of phase equilibria studies are shown in Table 2 and Figs. 8–10.

Fig. 6 shows SEM images of coexisting phases for equilibrated mixtures at each targeted temperature, 1500, 1550, and 1600 °C. They are the results of experimental number 11 to 16 as shown in Tables 1 and 2 Two immiscible monoxide phases (monoxide #1 and #2) and one zincite equilibrium phase were observed at 1500 and 1550 °C, as shown in Fig. 6 (a) and (b), respectively. At 1600 °C, two immiscible monoxide phases and one slag phase were observed. In the center of samples, the monoxide #1 phase were surrounded by liquid slag phase, while the monoxide #2 were located at the edge of samples, as shown in Fig. 6 (c) and (d). The slag phase was rarely observed at 1550 °C as shown in Fig. 6 (b). It could exist because of the eutectic point of the CaO–ZnO system at 1535 °C as shown in Fig. 3, as well as it is also expected as shown in Fig. 9. The expected equilibrated composition of slag was around 0.3CaO-0.1MgO-0.6ZnO, marked as circle in gray. However, the final equilibrated compositions were monoxide #2 and zincite. It is assumed that the Slag and Slag + Monoxide #1 (S + M#1) phases' areas are narrower than other phases in the expected phase diagram in Fig. 9. It indicates that the liquid slag phase could be unstable, so its phase was changed to monoxide or zincite phase. Therefore, the slag phase at 1550 °C was not considered as an equilibrium phase. In fact, the slag phase at 1550 °C in Fig. 6(b) existed in a limited area comparing the slag phase at 1600 °C that widely and evenly exists as shown Fig. 6 (c) and (d).

Fig. 7 shows SEM images of phase equilibria for equilibrium lines on the CaO–MgO–ZnO system at 1500 °C. The compositions of equilibrated phases were expected to fit well along the equilibrium line of two different phases as shown in Fig. 8, following the Gibbs phase rule (F = C–P+2). In the phase diagram of Fig. 8, the F is C–P, due to diagram as iso-baric (1atm) and iso-thermal (1550 °C) states. Therefore, if 2 phases are observed, the composition would follow the equilibrium line of the two different phases (F = 3–2 = 1). In practice, the SEM/EDS results show that there are two equilibrated phases, such as two immiscible monoxide or monoxide and zincite phases as shown in Fig. 7 and Table 2. The equilibrated compositions were marked as closed symbols on the phase diagram in Fig. 8. They also fit well along the equilibrium lines. Interestingly, several tiny and small un-equilibrated phases in white circles were observed in Fig. 7 (a) and (b). Their compositions were marked as half-closed shape and fit quite well the tie line of two immiscible monoxides as shown in Fig. 8. This proves that the equilibrium's mechanism is followed the direction of the tie lines between two different phases.

Fig. 8 shows optimized phase diagram of the ternary CaO–MgO–ZnO system at 1500 °C. The initial composition was set as the opened symbols in the Figure, while the compositions of equilibrium phases are shown as closed symbols. The half-closed symbols indicate un-equilibrated composition on the tie-lines as explained the above. As shown in Fig. 8, the new optimized (solid lines) was optimized following the phase equilibria studies. Also, the new lines were compared to the present Factsage 8.1 calculation by its own database, FToxid (dot lines). The new lines show more bigger triangle area of two immiscible monoxide and zincite phase (M#1+M#2+Z). The new lines fit well equilibrated compositions, and the values of the optimized parameters are shown in Table 3.

Fig. 9 shows optimized phase diagram of the ternary CaO–MgO–ZnO system at 1550 °C. The new optimized phase diagram shows a liquid slag phase exist, as shown in Fig. 6 (b), while the calculation from Factsage database shows solid phases without the liquid phases. This liquid phase is considered to be derived from the new optimized the CaO–ZnO system having the eutectic point at 1535 °C, as shown in Fig. 5. Even though the initial compositions were set in two different areas (S + M#1+M#2 and S + M#1+Z) to figure out coexisting phases for equilibrated mixtures including slag phases, the results expectedly showed the equilibrated monoxide or zincite phase as explained the above. The new lines fit well equilibrated compositions, and the values of the optimized parameters

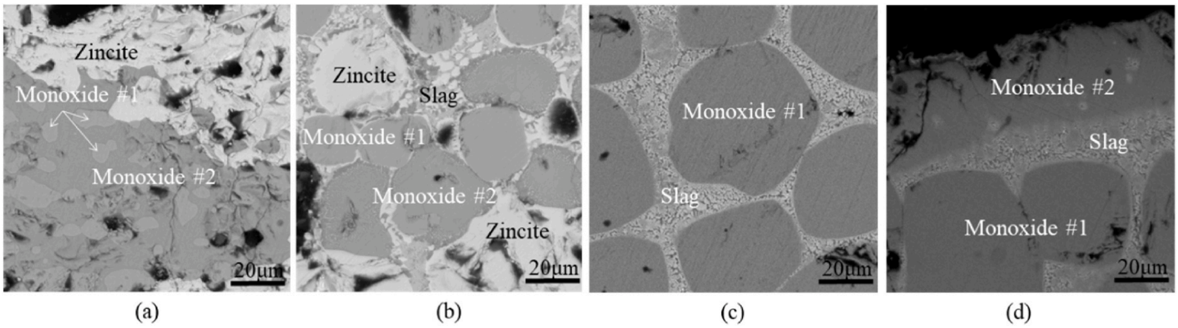

(a) (b) (c) (d)

Fig. 6. SEM image of coexisting phases for equilibrated mixtures of the ternary CaO–MgO–ZnO systems (a) at 1500 °C (b) at 1550 °C (c) at 1600 °C (center of sample) (d) at 1600 °C (edge of sample).

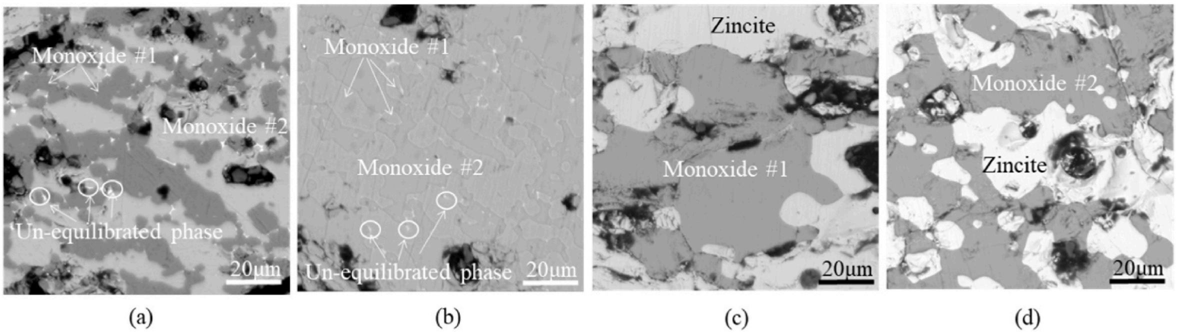

Fig. 7. SEM images of phase equilibria studies of the ternary CaO–MgO–ZnO system at 1500 °C (a) 0.45CaO-0.45MgO-0.1ZnO (No. 7) (b) 0.375CaO-0.375MgO-0.25ZnO (No. 8) (c) 0.02CaO-0.35MgO-0.65ZnO (No. 9) (d) 0.4CaO-0.05MgO-0.45ZnO (No. 10).

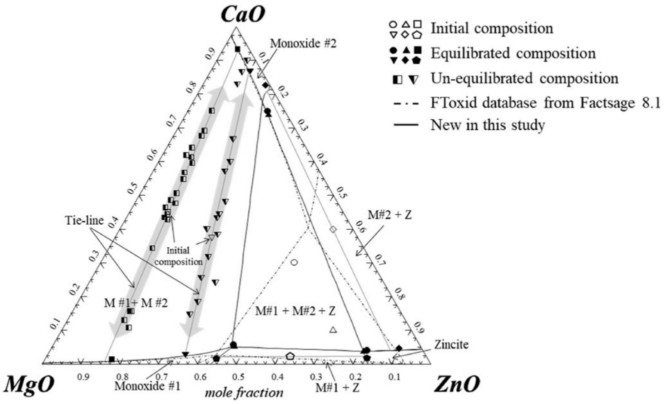

Fig. 8. Optimized phase diagram of the ternary CaO–MgO–ZnO system at 1500 °C. Experimental data from this study.

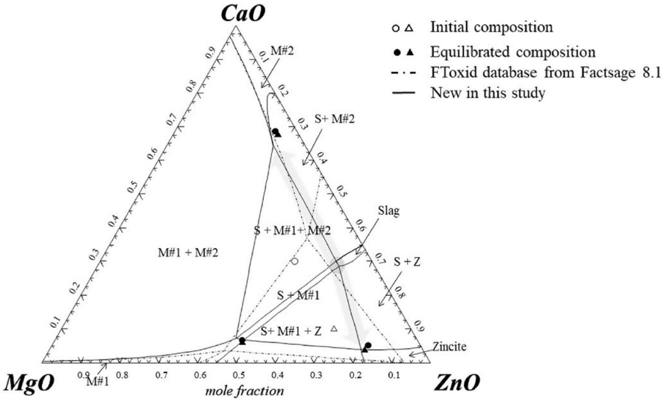

Fig. 9. Optimized phase diagram of the ternary CaO–MgO–ZnO system at 1550 °C. Experimental data from this study.

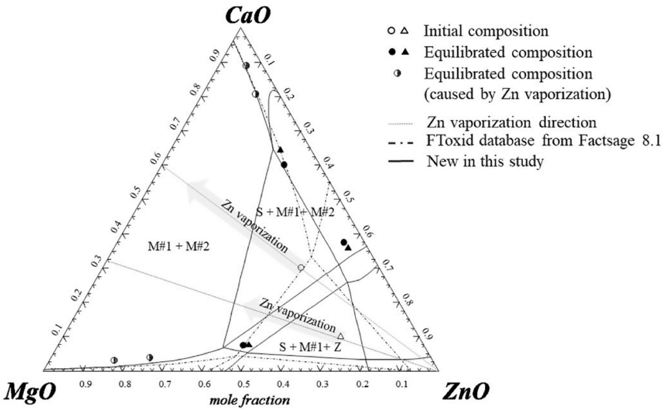

Fig. 10. Optimized phase diagram of the ternary CaO–MgO–ZnO system at 1600 °C. Experimental data from this study.

are shown in Table 3.

Fig. 10 shows CaO–MgO–ZnO optimized phase diagram at 1600 °C. It shows a similar shape to the phase diagram at 1550 °C, while the calculation from Factsage database shows solid solutions without liquid phases. The liquid slag phase has a larger stability field at 1600 °C than that of 1550 °C. This is derived from the expanded liquid slag phase area of the binary CaO–ZnO system at 1600 °C in Fig. 5. The phase equilibria experiment at 1600 °C were carried out with lower equilibration time (6 h) than those of 1500 and 1550 °C (10 h). However, the Zn vaporization occurred due to the higher temperature and higher stability of the slag phase. Hence, other equilibrated phases caused by Zn vaporization were also observed on the immiscible monoxide lines as shown in Fig. 10. An initial set of parameters were able to fit the phase equilibria of the ternary system at 1500 and 1550 °C based only on binary parameters. However, due to large stability of the liquid phase at 1600 °C, an additional ternary parameter was introduced to also fit the experimental data at 1600 °C. As the monoxide phases have larger stability fields in the phase diagram; thus, its ternary Gibbs excess energy parameter was optimized for monoxide phase, as mentioned in equation (4). For interpolation of binary parameters to the ternary system, CaO, MgO, and ZnO components are considered as similar, so the symmetric Kohler's interpolation model was introduced [30,33]. The new lines fit well equilibrated compositions, and the values of the optimized parameters are shown in Table 3.

Fig. 11(b) shows the optimized liquidus projection of the CaO–MgO–ZnO system. It shows different composition of the ternary eutectic point, and different shape areas of two immiscible monoxides and zincite phases, compared the calculation by Factsage FToxid database as show in Fig. 11(a). Also, Fig. 11(a) shows that the three phase monoxide#1-monoxide#2-liquid boundary line only extends to a minimum at around 1900 °C and that there is no invariant point consisting of two monoxides, zincite and liquid phase. In the FToxid database, the liquid is in equilibrium with a single monoxide phase at temperatures below 1900 °C, while the new optimized phase diagram shows the occurrence of a four phase invariant point, with the eutectic point being 0.3mol% CaO – 0.1mol% MgO – 0.6mol% ZnO at 1528.4 °C. With this phase diagram, the reasonable liquid area and compositions for pyrometallurgical processes, such as ZnO-containing fayalite (ZFS) slag, can be suggested. In order to make liquid slag phases for extracting CaO, MgO, and ZnO materials, 0.35mol%CaO–0.10mol%MgO–0.65mol% ZnO composition at 1600 °C can be considered.

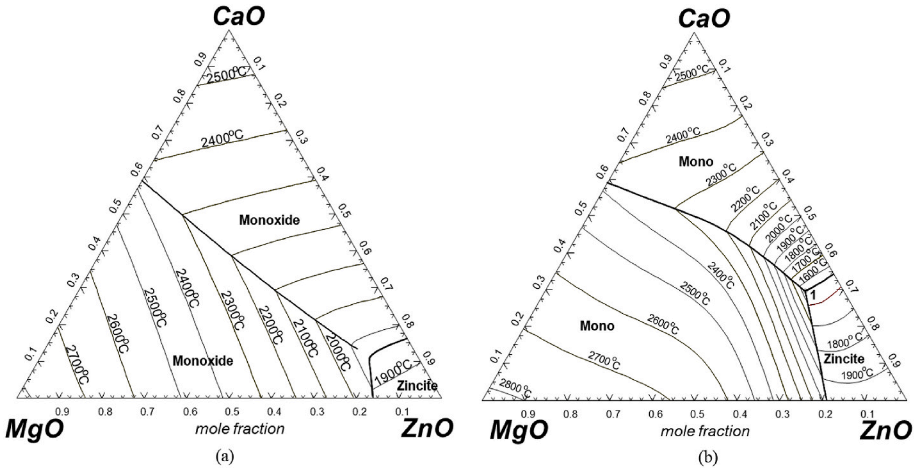

(a)

(b)

Fig. 11. Liquidus lines of the ternary CaO–MgO–ZnO system. (a) FToxid database from Factsage 8.1 [26] (b) Optimized lines from this study.

5. Conclusions

The binary MgO–ZnO and CaO–ZnO systems and the ternary CaO–MgO–ZnO system were thermodynamically optimized with phase equilibria studies in this study. The Bragg-Williams model used for all solid solutions, and Modified Quasichemical Model was used for the liquid phase. The optimized metastable Gibbs energies of MgO and CaO in zincite structure, and ZnO in monoxide structure were introduced. Optimized phase diagram fit well with phase equilibria studies. In particular, it was confirmed that the evolution of the composition of the immiscible monoxide phases follow the equilibrium tie lines in the CaO–MgO–ZnO system at 1500 °C. Liquid phases were newly observed in the CaO–MgO–ZnO systems at 1550 °C and 1600 °C. In the pyrometallurgical processes, the optimized phase diagrams can be applied to predict liquid phase of the ternary CaO–MgO–ZnO systems.

Declaration of competing interest

The authors declare that they have no known competing financial interests or personal relationships that could have appeared to influence the work reported in this paper.

Acknowledgments

Funding from the The Technology Industries of Finland Centennial Foundation - Steel and Metal Producers' Fund is greatly appreciated. This study utilized the Academy of Finland's RawMatTERS Finland Infrastructure (RAMI), based jointly at Aalto University, GTK, and VTT.

References

[1] B. Nourozi, A. Aminian, N. Fili, Y. Zangeneh, A. Boochani, P. Darabi, The electronic and optical properties of MgO mono-layer: based on GGA-mBJ, Results Phys. 12 (2019) 2038–2043, https://doi.org/10.1016/j.rinp.2019.02.054.

[2] A. Janotti, C.G. Van de Walle, Fundamentals of zinc oxide as a semiconductor, Rep. Prog. Phys. 72 (2009), 126501, https://doi.org/10.1088/0034-4885/72/12/126501.

[3] D.K. Nguyen, V.V. On, D.M. Hoat, J.F. Rivas-Silva, G.H. Cocoletzi, Structural, electronic, magnetic and optical properties of CaO induced by oxygen incorporation effects: a first- principles study, Phys. Lett. 397 (2021), 127241, https://doi.org/10.1016/j.physleta.2021.127241.

[4] J. Dagar, S. Castro-Hermosaa, G. Lucarelli, F. Cacialli, T.M. Brown, Highly efficient perovskite solar cells for light harvesting under indoor illumination via solution processed SnO_2/MgO composite electron transport layers, Nano Energy 49 (2018) 290–299, https://doi.org/10.1016/j.nanoen.2018.04.027.

[5] G. Wisz, I. Virt, P. Sagan, P. Potera, R. Yavorskyi, Structural, optical and electrical properties of zinc oxide layers produced by pulsed laser deposition method, Nanoscale Res. Lett. 12 (2017) 253, https://doi.org/10.1186/s11671-017-2033-9.

[6] S. Bai, J. Sun, Z. Zhou, C. Bu, X. Chen, Y. Yang, R. Wang, Y. Guo, C. Zhao, W. Liu, Structurally improved, TiO_2-incorporated, CaO-based pellets for thermochemical energy storage in concentrated solar power plants, Sol. Energy Mater. Sol. Cells 226 (2021), 111076, https://doi.org/10.1016/j.solmat.2021.111076.

[7] A. Sarkar, B. Breitung, H. Hahn, High entropy oxides: the role of entropy, enthalpy and synergy, Scripta Mater. 187 (2020) 43–48, https://doi.org/10.1016/j.scriptamat.2020.05.019.

[8] C.M. Rost, E. Sachet, T. Borman, A. Moballegh, E.C. Dickey, D. Hou, J.L. Jones, S. Curtarolo, J.-P. Maria, Entropy-stabilized oxides, Nat. Commun. (2015), https://doi.org/10.1038/ncomms9485.

[9] A. Shahraki, S. Ghasemi-kahrizsangi, A. Nemati, Performance improvement of MgO-CaO refractories by the addition of nano-sized Al_2O_3, Mater. Chem. Phys. 198 (2017) 354–359.

[10] J. Yang, X. Duan, L. Liu, H. Yang, X. Jiang, Recovery of magnesium from ferronickel slag to prepare magnesium oxide by sulfuric acid leaching, Minerals 11 (2021) 1375, https://doi.org/10.3390/min11121375.

[11] A. Ma, X. Zheng, S. Li, Y. Wang, S. Zhu, Zinc recovery from metallurgical slag and dust by coordination leaching in NH_3–CH_3COONH_4–H_2Osystem, R. Soc. Open Sci. 5 (2018), 180660, https://doi.org/10.1098/rsos.180660.

[12] M. Owais, R.M. Yazdani, M. Järvinen, Wet extractive grinding process for efficient calcium recovery from steelmaking slags, Chem. Eng. Process 151 (2020), 107917, https://doi.org/10.1016/j.cep.2020.107917.

[13] L. Chen, M. Guo, H. Shi, S. Huang, P.T. Jones, B. Blanpain, A. Malfliet, Effect of ZnO level in secondary copper smelting slags on slag/magnesia-chromite refractory interactions, J. Eur. Ceram. Soc. 36 (2016) 1821–1828, https://doi.org/10.1016/j.jeurceramsoc.2016.02.004.

[14] B. Gorai, R.K. Jana, Premchand, Characteristics and utilisation of copper slag-a review, Resour. Conserv. Recycl. 39 (2003) 299–313, https://doi.org/10.1016/S0921-3449(02)00171-4.

[15] A. Fallah-Mehrjardi, P.C. Hayes, E. Jak, The effect of CaO on gas/slag/matte/tridymite equilibria in fayalite-based copper smelting slags at 1473 K (1200 °C) and P(SO2) = 0.25 atm, Metall. Mater. Trans. B 48 (2018) 602–609, https://doi.org/10.1007/s11663-018-1170-6.

[16] P.J. Spencer, A brief history of CALPHAD, Calphad 320 (2008) 1–8, https://doi.org/10.1016/j.calphad.2007.10.001.

[17] I.-H. Jung, M.-A. Van Ende, Computational thermodynamic calculations: FactSage from CALPHAD thermodynamic database to virtual process simulation, Metall. Mater. Trans. B 51 (2020) 1851–1874, https://doi.org/10.1007/s11663-020-01908-7.

[18] L. Xia, Z. Liu, P. Taskinen, Solubility study of the halite and wurtzite solid solutions in the MgO-ZnO system within temperature range from 1000 to 1600 °C, J. Alloys Compd. 687 (2016) 827–832, https://doi.org/10.1016/j.jallcom.2016.06.191.

[19] J.F. Sarver, F.L. Katnack, F.A. Hummel, Phase equilibria and manganese-activated fluorescence in the system $Zn_3(PO_4)_2$-$Mg_3(PO_4)_2$, J. Electrochem. Soc. 106 (1959) 960–963.

[20] E.R. Segnit, A.E. Holland, The system MgO-ZnO-SiO_2, J. Am. Ceram. Soc. 48 (1965) 409–413, https://doi.org/10.1111/j.1151-2916.1965.tb14778.x.

[21] S. Raghavan, J.P. Hajra, G.N.K. Iyengar, K.P. Abraham, Terminal solid solubilities at 900- 1000°C in the magnesium oxide-zinc oxide system measured using a magnesium fluoride solid-electrolyte galvanic cell, Thermochim. Acta 189 (1991) 151–158, https://doi.org/10.1016/0040-6031(91)87109-A.

[22] D.S. Kenny, A. Navrotsky, Approximate activity-composition relations in the system MgO- ZnO at 1205 ± 5°C, J. Inorg. Nucl. Chem. 34 (1972) 2115–2119, https://doi.org/10.1016/0022-1902(72)80142-8.

[23] L. Xia, Z. Liu, P. Taskinen, Phase equilibrium study of the CaO–ZnO system, J. Am. Ceram. Soc. 99 11 (2016) 3809–3815, https://doi.org/10.1111/jace.14405.

[24] M. ShevchenkoM, E. Jak, Thermodynamic optimization of the binary CaO–ZnO and ternary CaO–ZnO–SiO_2 systems, Calphad 70 (2020), 101800, https://doi.org/10.1016/j.calphad.2020.101800.

[25] P. Wu, G. Eriksson, A.D. Pelton, Critical evaluation and optimization of the thermodynamic properties and phase diagrams of the CaO–FeO, CaO–MgO,

CaO–MnO, FeO–MgO, FeO– MnO, and MgO–MnO systems, J. Am. Ceram. Soc. 76 I (1993) 2065–2075, https://doi.org/10.1111/j.1151-2916.1993.tb08334.x.
[26] A.D. Pelton, Ber. Bunsenges. Phys. Chem. 84 (1980) 212–238, https://doi.org/10.1002/bbpc.1980084030.
[27] version 8.1, www.factsage.com.
[28] A.D. Pelton, Y.-B. Kang, Modeling short-range ordering in solutions, Int. J. Math. Res. 98 10 (2007) 907–917, https://doi.org/10.3139/146.101554.
[29] A.D. Pelton, S.A. Degterov, G. Eriksson, C. Robelin, Y. Dessureault, The modified quasichemical model I—binary solutions, Metall. Mater. Trans. B 31 (2000) 651–659, https://doi.org/10.1007/s11663-000-0103-2.
[30] A.D. Pelton, Phase Diagrams and Thermodynamic Modeling of Solutions, Elsevier, 2019, https://doi.org/10.1016/B978-0-12-801494-3.09994-2.
[31] M.A. Abramson, C. Audet, G. Couture, J.E. Dennis Jr., S. Le Digabel, Gerad. www.gerad.com/nomad.
[32] E. Königsberger, G. Eriksson, A new optimization routine for chemsage, Calphad 19 (1995) 207–214, https://doi.org/10.1016/0364-5916(95)00021-6.
[33] A.D. Pelton, A general "geometric" thermodynamic model for multicomponent solutions, Calphad 25 2 (2001) 319–328, https://doi.org/10.1016/S0364-5916(01)00052-9.